Non-Perturbative Dilepton Production from a Quark-Gluon Plasma *

Munshi G. Mustafa[1†], Andreas Schäfer[2], and Markus H. Thoma[1‡]
[1] *Institut für Theoretische Physik, Universität Giessen, 35392 Giessen, Germany*
[2] *Institut für Theoretische Physik, Universität Regensburg, 93040 Regensburg*
(October 9, 1999)

Abstract

The dilepton production rate from the quark-gluon plasma is calculated from the imaginary part of the photon self energy using a quark propagator that contains the gluon condensate. The low mass dilepton rate obtained in this way exhibits interesting structures (peaks and gaps), which might be observable at RHIC and LHC.

PACS numbers: 12.38.Mh, 12.38.Lg, 25.75.-q

Typeset using REVTEX

*Supported by BMBF, GSI Darmstadt, DFG, and Humboldt foundation

†Humboldt fellow and on leave from Saha Institute of Nuclear Physics, 1/AF Bidhan Nagar, Calcutta 700 064, India

‡Heisenberg fellow

I. INTRODUCTION

Thermal dileptons emitted from the fireball in ultrarelativistic heavy ion collisions might serve as a promising signature for the quark-gluon (QGP) formation in such collisions [1]. In contrast to hadronic signals dileptons and photons carry direct information about the early phase of the fireball, since they do not interact with the surrounding medium after their production [2]. Therefore they can be used as a direct probe for the QGP. Unfortunately there is a huge background coming from hadronic decays. Hence it would be desirable to have some specific features in the dilepton spectrum which could signal the presence of deconfined matter. Indeed perturbative calculations [3,4] have shown distinct structures (van Hove singularities, gaps) in the production rate of low mass dileptons caused by non-trivial in-medium quark dispersion relations. Unfortunately such calculations are not reliable at temperatures within reach of heavy ion collisions, where the coupling constant is not small. Moreover, perturbative calculations of the dilepton rate seem not to converge even in the small coupling limit [5].

Lattice QCD, on the other hand, is not capable so far to compute dynamical quantities such as the dilepton production rate. However, lattice calculations provide clear evidence for the existence of non-perturbative effects, e.g. effective parton masses [6], hadronic correlators [7], and the gluon condensate [8], above the phase transition. Recently QCD Green functions at finite temperature, which take the presence of a gluon condensate in the QGP into account [9,10], have been constructed.

In the present paper we will study the influence of this non-perturbative effect on the dilepton production rate. For this purpose, we will calculate the dilepton rate from the imaginary part of the photon self energy using an effective quark propagator that contain the gluon condensate. We will find similar structures as in the perturbative case coming from the quark dispersion relation which follows from the pole of the effective quark propagator. These structures might serve as an unique signature for the presence of deconfined, collective quarks in ultrarelativistic heavy ion collisions.

In the next section we will shortly review the basic ideas and results for the thermal quark propagator in the presence of a gluon condensate. In section 3 we will present our calculations of the dilepton production rate, before we will discuss our results in section 4.

II. QUARK PROPAGATION AND GLUON CONDENSATE

The effective quark propagator follows from the quark self energy containing the gluon condensate [9,11]. The following gauge independent result for this propagator at finite temperature has been found:

$$\tilde{S}(L) = \frac{\gamma_0 - \hat{l}\cdot\vec{\gamma}}{2D_+(L)} + \frac{\gamma_0 + \hat{l}\cdot\vec{\gamma}}{2D_-(L)} \ , \tag{1}$$

where

$$D_\pm(L) = (-l_0 \pm l)(1+a) - b, \tag{2}$$

and L is the fermionic four-momentum defined as $L = (l_0, \vec{l})$. The expressions for a and b are obtained in terms of the chromoelectric and chromomagnetic condensates as [9]

$$a = -\frac{g^2}{6}\frac{1}{L^6}\left[\left(\frac{1}{3}l^2 - \frac{5}{3}l_0^2\right)\langle\mathcal{E}^2\rangle_T - \left(\frac{1}{5}l^2 - l_0^2\right)\langle\mathcal{B}^2\rangle_T\right],$$
$$b = -\frac{4}{9}g^2\frac{l_0}{L^6}\left[l_0^2\langle\mathcal{E}^2\rangle_T + \frac{1}{5}l^2\langle\mathcal{B}^2\rangle_T\right], \qquad (3)$$

where $g^2 = 4\pi\alpha_s$. The in-medium chromoelectric, $\langle\mathcal{E}^2\rangle_T$, and chromomagnetic condensates, $\langle\mathcal{B}^2\rangle_T$, come from the non-perturbative longitudinal and transverse gluon propagators entering the quark self energy [9]. In Minkowski space these condensates can be expressed in terms of the space like (Δ_σ) and time like (Δ_τ) plaquette expectation values measured on a lattice [8] by [9]

$$\frac{\alpha_s}{\pi}\langle\mathcal{E}^2\rangle_T = \frac{4}{11}T^4\Delta_\tau - \frac{2}{11}\langle G^2\rangle_{T=0}\ ,$$
$$\frac{\alpha_s}{\pi}\langle\mathcal{B}^2\rangle_T = -\frac{4}{11}T^4\Delta_\sigma + \frac{2}{11}\langle G^2\rangle_{T=0}\ . \qquad (4)$$

The plaquette expectation values are related to the gluon condensate above T_c by [8,12]

$$\langle G^2\rangle_T = \langle G^2\rangle_{T=0} - \Delta T^4\ , \qquad (5)$$

where the interaction measure $\Delta = \Delta_\sigma + \Delta_\tau$ and $\langle G^2\rangle_{T=0} = (2.5 \pm 1.0)T_c^4$.

The dispersion relation of a quark interacting with the thermal gluon condensate is given by the roots of $D_\pm(L) = 0$ (2). The functions a and b (3) in (2) have been determined by using (4), where we took the plaquette expectation values from the lattice calculations of Ref. [8]. In Figs.1-3 we have displayed the dispersion relation of a quark having momentum l for $T = 1.1\ T_c$, $2\ T_c$ and $4\ T_c$, respectively. As shown in these figures there are two real positive solutions of $D_\pm(L) = 0$. For a given T the upper curve $\omega_+(l)$ corresponds to the solution of $D_+(L) = 0$, whereas the lower curve $\omega_-(l)$ represents the solution of $D_-(L) = 0$. Both branches are situated above the free dispersion relation $\omega = l$, and start from a common effective mass obtained in the $l \to 0$ limit as [9]

$$\omega_+(0) = \omega_-(0) = m_{\rm eff} = \left[\frac{2\pi\alpha_s}{3}\left(\langle\mathcal{E}^2\rangle_T + \langle\mathcal{B}^2\rangle_T\right)\right]^{1/4}\ , \qquad (6)$$

which is given by $m_{\rm eff} \approx 1.15\ T$ between $T = 1.1\ T_c$ and $4\ T_c$. The dispersion relation of a quark interacting with the in-medium gluon condensate is similar to the dispersion relation obtained from the hard thermal loop resummed (HTL) quark propagator [3]. The $\omega_+(l)$ branch describes the propagation of an ordinary quark with thermal mass, and as in the HTL case we denote this quasiparticle by q_+, as the ratio of its chirality to helicity is $+1$. For large momenta it is given by $\omega_+ = l + c_1$, where c_1 is a constant containing the condensate [9]. On the other hand, the $\omega_-(l)$ branch corresponds to the propagation of a quark mode with a negative chirality to helicity ratio. This branch represents the plasmino mode which is absent in the vacuum, and we denote this quasiparticle by q_-. As in the HTL case the $\omega_-(l)$ branch (plasmino mode) has a shallow minimum. For temperatures up to $2\ T_c$ this plasmino branch rapidly approaches the free dispersion relation (Figs.1 and 2). Owing to the strong increase of the magnetic condensate above $2\ T_c$ the plasmino branch stays clearly above the free dispersion relation for momenta under consideration (see Fig.3). For high momenta, however, this branch approaches the free dispersion relation, $\omega_- \to l$. The

plasmino mode corresponds to a purely collective long wave-length mode [3]. The residue of its pole being proportional to $(\omega_-^2 - l^2)^3$ for large momenta, becomes negligible for $l \gg T$. As a possible application of these quasiparticles dispersion relations, we will study the dilepton production from a quark-gluon plasma. As we shall see below these dispersion relations will cause peaks in the dilepton production rate, which could provide a possible signature of a quark-gluon plasma produced in heavy ion collisions.

III. DILEPTON PRODUCTION

The dilepton production rate calculated from the photon self energy in the case of one massless lepton flavor is given by

$$\frac{\mathrm{d}R}{\mathrm{d}^4x\mathrm{d}^4P} = -\frac{1}{12\pi^4}\frac{\alpha}{M^2}\frac{1}{e^{E/T}-1}\mathrm{Im}\Pi^\mu_\mu(P), \tag{7}$$

where $E = \sqrt{p^2+M^2}$ is the energy of the photon with invariant mass M.

Within the one-loop approximation the photon self energy (Fig.4) can be written using the Matsubara technique as

$$\Pi^{\mu\nu}(P) = -\frac{10}{3}e^2T\sum_{k_0}\int\frac{\mathrm{d}^3k}{(2\pi)^3}\mathrm{Tr}\left[\tilde{S}(K)\gamma^\mu\tilde{S}(Q)\gamma^\nu\right], \tag{8}$$

where K and $Q = P - K$ are the fermionic loop four-momenta. In the following only massless u and d quarks are considered. We want to study the effect of an in-medium gluon condensate on the production rate of lepton pairs. This effect can be included by using effective propagators containing the gluon condensate for the exchanged quarks. In view of this we have replaced the bare propagators by the effective propagators[1] in (8) as indicated by the filled circles in Fig.4.

Substitution of (1) in (8) and performing the traces yields [13]

$$\begin{aligned}\Pi^\mu_\mu(P) = \frac{10}{3}e^2T\sum_{k_0}\int\frac{\mathrm{d}^3k}{(2\pi)^3}\Bigg[&\frac{1}{D_+(K)}\left(\frac{1-\hat{k}\cdot\hat{q}}{D_+(Q)}+\frac{1+\hat{k}\cdot\hat{q}}{D_-(Q)}\right)\\ &+\frac{1}{D_-(K)}\left(\frac{1+\hat{k}\cdot\hat{q}}{D_+(Q)}+\frac{1-\hat{k}\cdot\hat{q}}{D_-(Q)}\right)\Bigg]\ .\end{aligned} \tag{9}$$

Now the imaginary part of the self energy can be computed by introducing spectral functions for the effective quark propagators as in the case of the real photon rate [13]. Following this work the imaginary part of (9) can be expressed as

$$\begin{aligned}\mathrm{Im}\Pi^\mu_\mu(P) = -\frac{10\pi}{3}e^2\left(e^{E/T}-1\right)\int\frac{\mathrm{d}^3k}{(2\pi)^3}\int_{-\infty}^{\infty}\mathrm{d}\omega\int_{-\infty}^{\infty}\mathrm{d}\omega'\\ \times\delta\left(E-\omega-\omega'\right)n_F(\omega)n_F(\omega')\\ \times\Big[\left(1+\hat{q}\cdot\hat{k}\right)\left\{\rho_+\left(\omega,k\right)\rho_-\left(\omega',q\right)+\rho_-\left(\omega,k\right)\rho_+\left(\omega',q\right)\right\}\\ +\left(1-\hat{q}\cdot\hat{k}\right)\left\{\rho_+\left(\omega,k\right)\rho_+\left(\omega',q\right)+\rho_-\left(\omega,k\right)\rho_-\left(\omega',q\right)\right\}\Big],\end{aligned} \tag{10}$$

[1]The additional use of an effectice quark-photon vertex will be discussed below.

where n_F is the Fermi-Dirac distribution and $\rho_\pm$ are the spectral functions corresponding to $1/D_\pm(L)$ given by

$$\rho_\pm(\omega,l) = R_\pm(\omega,l)\delta\left(\omega-\omega_\pm\right) + R_\mp(-\omega,l)\delta\left(\omega+\omega_\mp\right) \ , \tag{11}$$

where

$$R_\pm = \left|\frac{\left(\omega^2-l^2\right)^3}{C_\pm}\right| \tag{12}$$

with

$$\begin{aligned} C_\pm = -\Bigg[&(1+a)\left(\omega^2-l^2\right)^3 \ + \ \frac{b\left(\omega^2-l^2\right)^3}{\omega} \ + \ 6\omega(\omega\mp l)(\omega^2-l^2)^2 \\ &+ \ \frac{g^2}{3}\omega(\omega\mp l)\left(\frac{5}{3}\langle\mathcal{E}^2\rangle_T - \langle\mathcal{B}^2\rangle_T\right) \ - \ \frac{8}{9}g^2\omega^2\langle\mathcal{E}^2\rangle_T\Bigg]. \end{aligned} \tag{13}$$

The spectral functions in (11) contain only contributions from the poles of the effective propagator corresponding to the solutions $\omega_\pm$ of the dispersion relation $D_\pm(L)=0$ of the collective quark modes. They do not have a contribution from discontinuities, corresponding to Landau damping [14], because the effective quark propagator (1) does not have an imaginary part coming from the quark self energy.

Inserting (11) into (10) and performing the ω-integrations, exploiting the delta functions of the spectral functions, one finds ($x=\hat{p}\cdot\hat{k}$)

$$\begin{aligned} \mathrm{Im}\Pi^\mu_\mu(P) = -\frac{5}{6\pi}e^2\left(e^{E/T}-1\right)\int_0^\infty \mathrm{d}k\,k^2\int_{-1}^{+1}\mathrm{d}x \\ \times\left[\left(1 \ + \ \hat{q}\cdot\hat{k}\right)A \ + \ \left(1 \ - \ \hat{q}\cdot\hat{k}\right)B\right], \end{aligned} \tag{14}$$

where

$$\begin{aligned} A = \ & n_F\left(\omega_+(k)\right) n_F\left(\omega_-(q)\right) R_+\left(\omega_+(k),k\right) R_-\left(\omega_-(q),q\right)\delta\left(E-\omega_+(k)-\omega_-(q)\right) \\ & + n_F\left(-\omega_-(k)\right) n_F\left(\omega_-(q)\right) R_-\left(\omega_-(k),k\right) R_-\left(\omega_-(q),q\right)\delta\left(E+\omega_-(k)-\omega_-(q)\right) \\ & + n_F\left(\omega_+(k)\right) n_F\left(-\omega_+(q)\right) R_+\left(\omega_+(k),k\right) R_+\left(\omega_+(q),q\right)\delta\left(E-\omega_+(k)+\omega_+(q)\right) \\ & + n_F\left(-\omega_-(k)\right) n_F\left(-\omega_+(q)\right) R_-\left(\omega_-(k),k\right) R_+\left(\omega_+(q),q\right)\delta\left(E+\omega_-(k)+\omega_+(q)\right) \\ & + n_F\left(\omega_-(k)\right) n_F\left(\omega_+(q)\right) R_-\left(\omega_-(k),k\right) R_+\left(\omega_+(q),q\right)\delta\left(E-\omega_-(k)-\omega_+(q)\right) \\ & + n_F\left(-\omega_+(k)\right) n_F\left(\omega_+(q)\right) R_+\left(\omega_+(k),k\right) R_+\left(\omega_+(q),q\right)\delta\left(E+\omega_+(k)-\omega_+(q)\right) \\ & + n_F\left(\omega_-(k)\right) n_F\left(-\omega_-(q)\right) R_-\left(\omega_-(k),k\right) R_-\left(\omega_-(q),q\right)\delta\left(E-\omega_-(k)+\omega_-(q)\right) \\ & + n_F\left(-\omega_+(k)\right) n_F\left(-\omega_-(q)\right) R_+\left(\omega_+(k),k\right) R_-\left(\omega_-(q),q\right)\delta\left(E+\omega_+(k)+\omega_-(q)\right) \end{aligned} \tag{15}$$

and

$$\begin{aligned} B = \ & n_F\left(\omega_+(k)\right) n_F\left(\omega_+(q)\right) R_+\left(\omega_+(k),k\right) R_+\left(\omega_+(q),q\right)\delta\left(E-\omega_+(k)-\omega_+(q)\right) \\ & + n_F\left(-\omega_-(k)\right) n_F\left(\omega_+(q)\right) R_-\left(\omega_-(k),k\right) R_+\left(\omega_+(q),q\right)\delta\left(E+\omega_-(k)-\omega_+(q)\right) \\ & + n_F\left(\omega_+(k)\right) n_F\left(-\omega_-(q)\right) R_+\left(\omega_+(k),k\right) R_-\left(\omega_-(q),q\right)\delta\left(E-\omega_+(k)+\omega_-(q)\right) \end{aligned}$$

$$
\begin{aligned}
&+ n_F\left(-\omega_-(k)\right) n_F\left(-\omega_-(q)\right) R_-\left(\omega_-(k),k\right) R_-\left(\omega_-(q),q\right) \delta\left(E+\omega_-(k)+\omega_-(q)\right) \\
&+ n_F\left(\omega_-(k)\right) n_F\left(\omega_-(q)\right) R_-\left(\omega_-(k),k\right) R_-\left(\omega_-(q),q\right) \delta\left(E-\omega_-(k)-\omega_-(q)\right) \\
&+ n_F\left(-\omega_+(k)\right) n_F\left(\omega_-(q)\right) R_+\left(\omega_+(k),k\right) R_-\left(\omega_-(q),q\right) \delta\left(E+\omega_+(k)-\omega_-(q)\right) \\
&+ n_F\left(\omega_-(k)\right) n_F\left(-\omega_+(q)\right) R_-\left(\omega_-(k),k\right) R_+\left(\omega_+(q),q\right) \delta\left(E-\omega_-(k)+\omega_+(q)\right) \\
&+ n_F\left(-\omega_+(k)\right) n_F\left(-\omega_+(q)\right) R_+\left(\omega_+(k),k\right) R_+\left(\omega_+(q),q\right) \delta\left(E+\omega_+(k)+\omega_+(q)\right).
\end{aligned}
\tag{16}
$$

Changing the integration variable from x to $q = |\vec{p}-\vec{k}| = \sqrt{p^2+k^2-2pkx}$ the dilepton production rate (7) can be written as

$$
\begin{aligned}
\frac{\mathrm{d}R}{\mathrm{d}^4x\mathrm{d}^4P} = \frac{5}{36\pi^4}\frac{\alpha^2}{M^2}\frac{1}{p}&\left[\int_0^p \mathrm{d}k \int_{p-k}^{p+k} \mathrm{d}q + \int_p^\infty \mathrm{d}k \int_{k-p}^{p+k} \mathrm{d}q\right] \\
&\times\left[\left(p^2-(k-q)^2\right)A + \left((k+q)^2-p^2\right)B\right].
\end{aligned}
\tag{17}
$$

Now one can perform the q-integration by means of the remaining δ-functions in A and B leading to

$$
\begin{aligned}
\frac{\mathrm{d}R}{\mathrm{d}^4x\mathrm{d}^4P} = \frac{5}{36\pi^4}\frac{\alpha^2}{M^2}\frac{1}{p}\int_0^\infty \mathrm{d}k &\left[\left(p^2-(k-q_s)^2\right)\left(A_1+A_2+A_3+A_5+A_6+A_7\right)\right. \\
&\left.+\left((k+q_s)^2-p^2\right)\left(B_1+B_2+B_3+B_5+B_6+B_7\right)\right]_{|p-k|\le q_s\le p+k},
\end{aligned}
\tag{18}
$$

where the $q_s = q_s(E)$ determined by the various δ-functions in (15) and (16) can assume two different values in the case of the plasmino branch due to the presence of the minimum and

$$
\begin{aligned}
A_1 &= n_F\left(\omega_+(k)\right) n_F\left(\omega_-(q_s)\right) R_+\left(\omega_+(k),k\right) \frac{R_-\left(\omega_-(q_s),q_s\right)}{|\mathrm{d}\omega_-(q)/\mathrm{d}q|_{q_s}}, \\
A_2 &= n_F\left(-\omega_-(k)\right) n_F\left(\omega_-(q_s)\right) R_-\left(\omega_-(k),k\right) \frac{R_-\left(\omega_-(q_s),q_s\right)}{|\mathrm{d}\omega_-(q)/\mathrm{d}q|_{q_s}}, \\
A_3 &= n_F\left(\omega_+(k)\right) n_F\left(-\omega_+(q_s)\right) R_+\left(\omega_+(k),k\right) \frac{R_+\left(\omega_+(q_s),q_s\right)}{|\mathrm{d}\omega_+(q)/\mathrm{d}q|_{q_s}}, \\
A_5 &= n_F\left(\omega_-(k)\right) n_F\left(\omega_+(q_s)\right) R_-\left(\omega_-(k),k\right) \frac{R_+\left(\omega_+(q_s),q_s\right)}{|\mathrm{d}\omega_+(q)/\mathrm{d}q|_{q_s}}, \\
A_6 &= n_F\left(-\omega_+(k)\right) n_F\left(\omega_+(q_s)\right) R_+\left(\omega_+(k),k\right) \frac{R_+\left(\omega_+(q_s),q_s\right)}{|\mathrm{d}\omega_+(q)/\mathrm{d}q|_{q_s}}, \\
A_7 &= n_F\left(\omega_-(k)\right) n_F\left(-\omega_-(q_s)\right) R_-\left(\omega_-(k),k\right) \frac{R_-\left(\omega_-(q_s),q_s\right)}{|\mathrm{d}\omega_-(q)/\mathrm{d}q|_{q_s}}, \\
B_1 &= n_F\left(\omega_+(k)\right) n_F\left(\omega_+(q_s)\right) R_+\left(\omega_+(k),k\right) \frac{R_+\left(\omega_+(q_s),q_s\right)}{|\mathrm{d}\omega_+(q)/\mathrm{d}q|_{q_s}}, \\
B_2 &= n_F\left(-\omega_-(k)\right) n_F\left(\omega_+(q_s)\right) R_-\left(\omega_-(k),k\right) \frac{R_+\left(\omega_+(q_s),q_s\right)}{|\mathrm{d}\omega_+(q)/\mathrm{d}q|_{q_s}}, \\
B_3 &= n_F\left(\omega_+(k)\right) n_F\left(-\omega_-(q_s)\right) R_+\left(\omega_+(k),k\right) \frac{R_-\left(\omega_-(q_s),q_s\right)}{|\mathrm{d}\omega_-(q)/\mathrm{d}q|_{q_s}},
\end{aligned}
$$

$$
\begin{aligned}
B_5 &= n_F\left(\omega_-(k)\right) n_F\left(\omega_-(q_s)\right) R_-\left(\omega_-(k),k\right) \frac{R_-\left(\omega_-(q_s),q_s\right)}{|\mathrm{d}\omega_-(q)/\mathrm{d}q|_{q_s}},\\
B_6 &= n_F\left(-\omega_+(k)\right) n_F\left(\omega_-(q_s)\right) R_+\left(\omega_+(k),k\right) \frac{R_-\left(\omega_-(q_s),q_s\right)}{|\mathrm{d}\omega_-(q)/\mathrm{d}q|_{q_s}},\\
B_7 &= n_F\left(\omega_-(k)\right) n_F\left(-\omega_+(q_s)\right) R_-\left(\omega_-(k),k\right) \frac{R_+\left(\omega_+(q_s),q_s\right)}{|\mathrm{d}\omega_+(q)/\mathrm{d}q|_{q_s}},
\end{aligned}
\tag{19}
$$

The group velocity factors in (19) follow from the dispersion relation, $D_\pm(L)=0$, of (2) as

$$
\frac{\mathrm{d}\omega_\pm(l)}{\mathrm{d}l} = \pm\frac{F_\pm\left(\omega_\pm(q),a,b,l\right)}{G_\pm\left(\omega_\pm(q),a,b,l\right)}\ , \tag{20}
$$

where

$$
\begin{aligned}
F_\pm &= (1+a)^2\left(\omega_\pm^2(l)-l^2\right)^3 \ \mp\ 6b\left(\omega_\pm^2(l)-l^2\right)^2 l \ \mp\ \frac{g^2}{6}b\left(\frac{2}{3}\langle\mathcal{E}^2\rangle_T-\frac{2}{5}\langle\mathcal{B}^2\rangle_T\right) l\\
&\pm\ \frac{8}{45}g^2\,(1+a)\,l\omega_\pm(l)\langle\mathcal{B}^2\rangle_T\ \ ,\\
G_\pm &= -\,(1+a)\,C_\pm\ ,
\end{aligned}
\tag{21}
$$

and a, b, and $C_\pm$ are given in (3) and (13), respectively. As we will see in the next section the group velocity leads to a characteristic feature of the dilepton rate.

In (18) we have dropped terms A_4, A_8, B_4 and B_8 as the corresponding δ-functions in (16) can never be satisfied by virtue of energy conservation since $\omega_\pm$ is always positive. Now, one can perform the k-integration in (18) numerically, and we find that the terms, which satisfy the energy conservation, correspond to various physical processes involving two quasiparticles with different momentum k and q.

However, before discussing our results, we would like to give the corresponding dilepton production rate for $\vec{p}=0$. For this purpose we combine (7) and (14) with $\vec{q}=-\vec{k}$ and obtain

$$
\begin{aligned}
\frac{\mathrm{d}R}{\mathrm{d}^4x\mathrm{d}^4P}(\vec{p}=0) = \frac{10}{9\pi^4}\frac{\alpha^2}{M^2}\int_0^\infty \mathrm{d}k\,k^2\Big[&n_F^2\left(\omega_+(k)\right)R_+^2\left(\omega_+(k)\right)\delta\left(E-2\omega_+(k)\right)\\
&+\ 2n_F\left(\omega_+(k)\right)n_F\left(-\omega_-(k)\right)R_+\left(\omega_+(k)\right)R_-\left(\omega_-(k)\right)\delta\left(E-\omega_+(k)+\omega_-(k)\right)\\
&+\ 2n_F\left(\omega_-(k)\right)n_F\left(-\omega_+(k)\right)R_+\left(\omega_+(k)\right)R_-\left(\omega_-(k)\right)\delta\left(E+\omega_+(k)-\omega_-(k)\right)\\
&+\ n_F^2\left(\omega_-(k)\right)R_-^2\left(\omega_-(k)\right)\delta\left(E-2\omega_-(k)\right)\Big]\ .
\end{aligned}
\tag{22}
$$

After performing the k-integration by means of the δ-functions, the expression for the dilepton rate at $\vec{p}=0$ becomes

$$
\begin{aligned}
\frac{\mathrm{d}R}{\mathrm{d}^4x\mathrm{d}^4P}(\vec{p}=0) = \frac{10}{9\pi^4}\frac{\alpha^2}{M^2}\sum_{k_s}k_s^2\Bigg[&n_F^2\left(\omega_+(k_s)\right)R_+^2\left(\omega_+(k_s)\right)\frac{1}{2}\left|\frac{\mathrm{d}\omega_+(k)}{\mathrm{d}k}\right|_{k_s}^{-1}\\
&+\ 2n_F\left(\omega_+(k_s)\right)n_F\left(-\omega_-(k_s)\right)R_+\left(\omega_+(k_s)\right)R_-\left(\omega_-(k_s)\right)\left|\frac{\mathrm{d}\left(\omega_+(k)-\omega_-(k)\right)}{\mathrm{d}k}\right|_{k_s}^{-1}
\end{aligned}
$$

$$+\ 2n_F\left(\omega_-(k_s)\right) n_F\left(-\omega_+(k_s)\right) R_+\left(\omega_+(k_s)\right) R_-\left(\omega_-(k_s)\right) \left|\frac{\mathrm{d}\left(\omega_-(k)-\omega_+(k)\right)}{\mathrm{d}k}\right|_{k_s}^{-1}$$

$$+\ n_F^2\left(\omega_-(k_s)\right) R_-^2\left(\omega_-(k_s)\right) \frac{1}{2}\left|\frac{\mathrm{d}\omega_-(k)}{\mathrm{d}k}\right|_{k_s}^{-1}\Bigg] \ . \qquad (23)$$

IV. RESULTS AND DISCUSSION

First we would like to discuss the dilepton production from a quark-gluon plasma at momentum $\vec{p} = 0$ of the virtual photon. The corresponding rate is given by (23). The different terms in (23) correspond to various physical processes involving two quasiparticles q_+ and q_- with same momentum k. The first term represents the annihilation process $q_+\bar{q}_+ \to \gamma^*$. The second term corresponds to $q_+ \to q_-\gamma^*$, a decay process from a q_+-mode to a plasmino plus a virtual photon. Energy conservation does not allow the process given by the third term ($q_- \to \bar{q}_+\gamma^*$). Finally, the fourth term corresponds to a process, $q_-\bar{q}_- \to \gamma^*$, i.e. annihilation of plasmino modes. The static differential rate of the aforementioned processes are displayed in Fig.5 for $T = 1.1\ T_c$ (solid line), $2\ T_c$ (dashed curve) and $4\ T_c$ (dotted curve). Similar to the HTL case [3] the partial rate in the presence of a gluon condensate shows peaks (van Hove singularities) at different invariant masses of the virtual photon. Below we discuss the contributions to the rate from each process in detail.

The channel, $q_+ \to q_-\gamma^*$, opens up at $M = 0$. This process continues up to $M = 1.01\ T_c$ for $T = 1.1\ T_c$, $M = 1.83\ T_c$ for $T = 2\ T_c$ and $M = 2.14\ T_c$ for $T = 4\ T_c$, respectively, where the first peak appears due to the vanishing group velocity $dE/dk = 0$ at the maximum $E = M = \omega_+(k) - \omega_-(k)$, since the density of states, which enters the rate (23), is inversely proportional to the group velocity.

The $q_+ \to q_-\gamma^*$ channel terminates at the peak, after which there is a gap because neither of the other processes is possible in this invariant mass regime. The size of the gap depends on the temperature. For $T = 1.1\ T_c$ it ranges from $M = 1.01\ T_c$ to $2.07\ T_c$, for $T = 2\ T_c$ from $M = 1.83\ T_c$ to $3.73\ T_c$, and for $T = 4\ T_c$ from $M = 2.14\ T_c$ to $8.76\ T_c$.

The process, $q_-\bar{q}_- \to \gamma^*$, starts at an energy which is twice the energy of the minimum of the plasmino branch, $E = M = 2\omega_-(k_{min})$. The diverging density of states at that point again causes a van Hove singularity. This process continues with increasing M but falls off very fast due to two reasons: i) as M increases the high energy plasmino modes come into the game and the corresponding square of the residue $R_-^2(\omega_-(k), k)$, to which the rate is proportional, becomes very small since it is proportional to $(\omega_-^2(k) - k^2)^3$, and ii) with increasing M the density of states decreases gradually.

At $M = E = 2\omega_+(k) \geq 2m_{\rm eff}$, the process, $q_+\bar{q}_+ \to \gamma^*$, shows up. As M increases, the contribution from this process grows and dominates over the plasmino annihilation process, resulting in a dip in the dilepton rate. For large M this annihilation process is solely responsible for the dilepton rate.

For $T = 4\,T_c$ the contribution from the plasmino annihilation is nearly as big as the q_+-$\bar{q}_+$-annihilation at the mass regime displayed in Fig.4 because of the fairly large deviation of the plasmino branch from the free dispersion relation. This is the reason why the dilepton rate

is almost flat at large masses in Fig.5. Only at very large invariant masses the contribution from q_--$\bar{q}_-$-annihilation will vanish.

The channel $q_+\bar{q}_- \to \gamma^*$, which contributes in the case of the HTL calculation [3], is absent here. This can be traced back to the fact that we did not take into account an effective quark-photon vertex. Using such a vertex, (9) does not hold anymore and terms containing $\delta(E-\omega_+(k)-\omega_-(k))$ show up in (22).

Comparing our rate to the HTL result [3] for realistic values of the strong coupling constant appearing in the HTL rate, e.g. $g = 2.5$, we observe that our rate is smaller by about a factor of 5 to 10 than the pole-pole contribution of the HTL calculation. At large M the HTL rate reduces to the Born rate [3,15]

$$\frac{\mathrm{d}R^{\mathrm{Born}}}{\mathrm{d}^4x\mathrm{d}^4P}(\vec{p}=0) = \frac{5\alpha^2}{36\pi^4}\left(e^{M/2T}+1\right)^{-2}\ , \tag{24}$$

which follows from the first term of (22) in the limit $\omega_+ \to k$ where $R_+^{HTL} \to 1$. In contrast, the rate given here does not reduce to the Born rate in the large M limit, since R_+ is given by 1/4 instead of 1 for infinite large momenta. This can be seen easily from (12) using the asymptotic form of the ω_+ branch, $\omega_0^+ \to k + c_1$, discussed in section 2. The fact that R_+, which enters the rate (22) quadratically, is always small causes the suppression of the rate compared to the HTL case. Another reason for our small rate might be the fact that we did not take into account an effective quark-photon vertex in our calculation. Neglecting this vertex in the HTL computation leads to a reduction of the dilepton rate by a factor 2 to 10 depending on M.

Furthermore, since the spectral densities of the effective quark propagator have no discontinuous parts there is no contribution from cuts as opposed to [3]. In the HTL case the cut contribution, which shows no dramatic structures, dominates over the pole-pole contribution and covers the peaks and gap of the latter completely.

Finally we turn to the dilepton rate at non-zero virtual photon momentum. The corresponding rate is given in (18). The processes corresponding to terms A_2, A_3, A_6, A_7, B_6 and B_7, namely transitions within a branch and transitions from the lower to the upper branch, do not contribute to the rate, because they are forbidden for timelike photons decaying into dileptons due to energy conservation [4]. The processes corresponding to A_1 and A_5 indicate annihilation between a quark (q_+) and a plasmino mode (q_-) with different momentum to a virtual photon with energy E, which were absent at $p = 0$. The process given by B_1 is the annihilation between a quark and antiquark ($q_+(k)\bar{q}_+(q) \to \gamma^*$), whereas B_5 corresponds to the annihilation ($q_-(k)\bar{q}_-(q) \to \gamma^*$) between two plasmino modes. The term B_2 corresponds to the decay process, $q_+(q) \to q_-(k)\gamma^*$, whereas B_3 to $q_+(k) \to q_-(q)\gamma^*$. The differential rate involving these processes are displayed in Figs.6-8 for virtual photon momenta $p = 1$ T_c, 2 T_c, and 3 T_c, respectively, at different temperatures, namely $T = 1.1$ T_c (solid line), 2 T_c (dashed line), and 4 T_c (dotted line).

For $p = 1$ T_c (Fig.6) the decay processes corresponding to terms B_2 and B_3 open up at $E(=\sqrt{p^2+M^2})$=1 T_c. These processes continue up to $E = 2.0$ T_c for $T = 1.1$ T_c, $E = 2.8$ T_c for $T = 2$ T_c, and $E = 3.3$ T_c for $T = 4$ T_c, respectively. The first peak at $p = 0$ is smeared out and a shoulder appears, which becomes more and more significant as temperature increases. At very low invariant masses the contribution from these decay processes to the rate is large caused by a very large density of states due to kinematical

reasons. With increasing E the density of states decreases and at the same time the residue of the plasmino mode falls off gradually. The interplay of these two quantities is responsible for the shoulder in the rate, which is more pronounced at higher T.

The process corresponding to the annihilation of two plasmino modes (term B_5) turns on at $E = 2.1\ T_c$ for $T = 1.1\ T_c$, $E = 3.6\ T_c$ for $T = 2\ T_c$, and $E = 8.7\ T_c$ for $T = 4\ T_c$, respectively, with a smoothened van Hove peak and falls off rapidly due to the reasons explained above. The annihilation processes involving a quark and a plasmino mode (terms A_1 and A_5) open up at $E = 2.4\ T_c$ for $T = 1.1\ T_c$, $E = 4.1\ T_c$ for $T = 2\ T_c$, and $E = 9.1\ T_c$ for $T = 4\ T_c$, respectively. With increasing E the contribution from this two processes falls off rapidly. As a result of the interplay of these processes a small bump or plateau appears in the dilepton production rate. The annihilation process involving a q_+ and a $\bar{q}_+$ (term B_1) opens up at $E = 3.1\ T_c$ for $T = 1.1\ T_c$, $E = 5.2\ T_c$ for $T = 2\ T_c$, and $E = 9.7\ T_c$ for $T = 4\ T_c$. As explained for $p = 0$, the contribution from this process grows and dominates over the other processes at large E. The dip and the second bumb for lower T come from the interplay of the decreasing processes involving plasminos and the increasing process involving only quark modes. For higher T these structures vanish as in the $p = 0$ case.

In Fig.7 we have displayed the results for $p = 2\ T_c$. The gap for $T = 4\ T_c$ becomes narrower whereas the gap disappears for $T = 1.1\ T_c$ and $2\ T_c$. For all T the decay processes begin at $E = 2\ T_c$ and continue up to $E = 3.0\ T_c$ for $T = 1.1\ T_c$, $E = 3.9\ T_c$ for $T = 2\ T_c$, and $E = 4.6\ T_c$ for $T = 4\ T_c$. For $T = 1.1\ T_c$ the annihilation process involving two plasmino modes opens up around $E = 2.3\ T_c$ and for $T = 2\ T_c$ at $E = 3.7\ T_c$, causing the gap to disappear. The process involving annihilation of a quark and a plasmino mode opens up around $E = 3.2\ T_c$ for $T = 1.1\ T_c$, leading to a deep dip in the dilepton rate. As E increases the rate falls off and is finally dominated gradually by the quark-antiquark annihilation process, causing a second dip around $E = 4.3\ T_c$. For $T = 2\ T_c$ the small kink around $E = 4\ T_c$ is due to the interplay of decay and annihilation processes involving plasminos. At this temperature the annihilation process between a quark and a plasmino mode becomes active and results in a dip at $E \simeq 4.5\ T_c$. Again the second dip around $E = 6.2\ T_c$ is due to the interplay of the usual annihilation process and annihilation processes involving plasminos. The overall feature for $T = 4\ T_c$ remains the same as that at $p = 1\ T_c$.

As a last example the partial dilepton production rate for $p = 3\ T_c$ is displayed in Fig.8 for $T = (1.1 - 4)\ T_c$. The features for $T = 1.1\ T_c$ are the same as at $p = 2\ T_c$ except that the different processes involved now open up at higher energies. For $T = 2\ T_c$ the quark-plasmino annihilation processes starts at around $E = 5.3\ T_c$ in such a way that the valley like shape in the rate turns into a deep pocket. As expected, the gap width for $T = 4\ T_c$ shrinks a bit. Now the dilepton rate immediately after the gap is rather flat as the contribution from annihilation process involving two plasmino modes has stabilized. At $E = 8.8\ T_c$ the step like structure in the rate is caused by the onset of the annihilation processes between a quark and a plasmino mode. The usual annihilation process begins only around $E = 11\ T_c$, which is not shown in the figure.

Finally we want to discuss the neglect of an effective quark-photon vertex and possible observable consequences of our results. Such a vertex, related by the Ward identity to the effective quark propagator, should be taken into account when calculating the photon self energy. As a matter of fact, in the case of π^+-π^--annihilation the consideration of the Ward

identity lead to a strong suppression of the dilepton production [16]. In contrast, taking into account the effective quark-photon vertex in the HTL calculation leads to an increase of the rate by a factor 2 to 10 depending on M. Unfortunately, the computation of the effective quark-photon vertex and the photon self energy with such a vertex will be very involved. However, the positions of the singularities and the gap is solely determined by the quark dispersion relation. Our main result is that non-perturbative quark dispersion relations in the QGP lead to sharp structures in the dilepton rate at the positions shown in Figs.5-8.

The absolute value of the rate is determined not only by the consideration of the effective quark-photon vertex but also by higher order damping effects which will broaden the peaks. Whether these structures can be seen in the dilepton spectrum or not depends on the amount of broadening of the peaks and on the smoothening of these structures by the space-time evolution of the fireball. Furthermore processes involving additional gluons such as Compton scattering [3] and bremsstrahlung [5], which lead to a smooth dilepton rate [3], and hadronic processes might cover up these structures. If, however, new structures will be observed in the low mass ($M < 1$ GeV) dilepton spectrum, they will provide a strong indication for the presence of deconfined, collective quarks in the QGP, in particular since the hadronic contribution to the dilepton rate is expected to be smooth due to medium effects [17]. As a matter of fact, this argument does not depend on a specific approximation scheme [18] as the general behavior (two branches, common effective mass, plasmino minimum, free dispersion at large momenta) of the quark dispersion agrees with the one shown in Fig.1-3 and found in Ref. [3]. Although such structures have not been observed so far due to the small life time of the QGP phase at SPS (if it exists at all) as indicated by hydrodynamical calculation [19], it will be worthwhile to look for new structures in the low mass dilepton spectrum (in particular at low photon momenta) at RHIC and LHC, where the thermal dilepton spectrum is expected to be dominated by the QGP phase.

ACKNOWLEDGMENTS

We are grateful to J. Engels for useful correspondence.

REFERENCES

[1] P.V. Ruuskanen, Nucl. Phys. **A544**, 169c (1992).
[2] M.H. Thoma, Phys. Rev D **51**, 862 (1995).
[3] E. Braaten, R.D. Pisarski, and T.C. Yuan, Phys. Rev. Lett. **64**, 2242 (1990).
[4] S.M.H. Wong, Z. Phys. C **53**, 465 (1992).
[5] P. Aurenche, F. Gelis, R. Kobes, and H. Zaraket, Phys. Rev. D **58**, 085003 (1998); P. Aurenche, F. Gelis, R. Kobes, and H. Zaraket, hep-ph/9903307.
[6] A. Peshier, B. Kämpfer, O.P. Pavlenko, and G. Soff, Phys. Lett. B **337**, 235 (1994); A. Peshier, B. Kämpfer, O.P. Pavlenko, and G. Soff, Phys. Rev. D **54**, 2399 (1996).
[7] G. Boyd, S. Gupta, F. Karsch, and E. Laermann, Z. Phys. C **64**, 331 (1994).
[8] G. Boyd et al., Nucl. Phys. **B469**, 419 (1996).
[9] A. Schäfer and M. H. Thoma, Phys. Lett. B **451**, 195 (1999).
[10] I. Schmidt and J.J. Yang, hep-ph/9906510.
[11] M. J. Lavelle and M. Schaden, Phys. Lett. B **208**, 419 (1988).
[12] H. Leutwyler, in Proc. Conf. QCD - 20 years later, Eds. P. M. Zerwas and H. A. Kastrup (World Scientific, Singapore,1993) p. 693.
[13] J. I. Kapusta, P. Lichard, and D. Seibert, Phys. Rev. D **44**, 2774 (1991).
[14] R. D. Pisarski, Physica A **158**, 146 (1989).
[15] J. Cleymans, J. Fingberg, and K. Redlich, Phys. Rev. D **35**, 2153 (1987).
[16] C.L. Korpa and S. Pratt, Phys. Rev. Lett. **64**, 1502 (1991).
[17] R. Rapp and J. Wambach, hep-ph/9907502.
[18] A. Peshier and M.H. Thoma, hep-ph/9907268.
[19] J. Sollfrank et al., Phys. Rev. C **55**, 392 (1997).

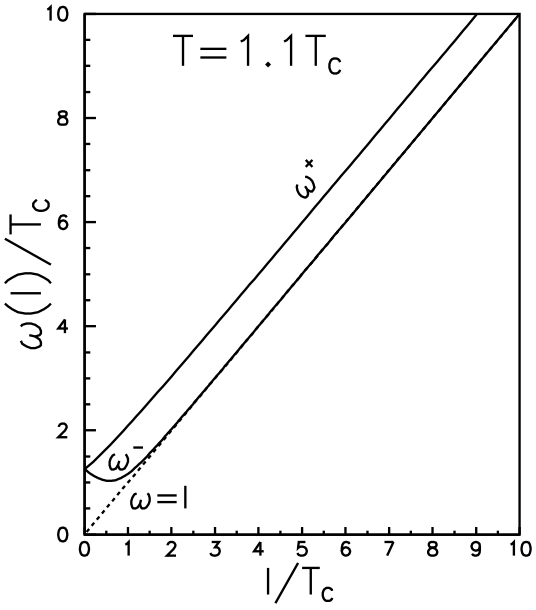

FIG. 1. Quark dispersion relation $\omega(l)/T_c$ versus l/T_c in a QGP at $T = 1.1\ T_c$ in the presence of a gluon condensate.

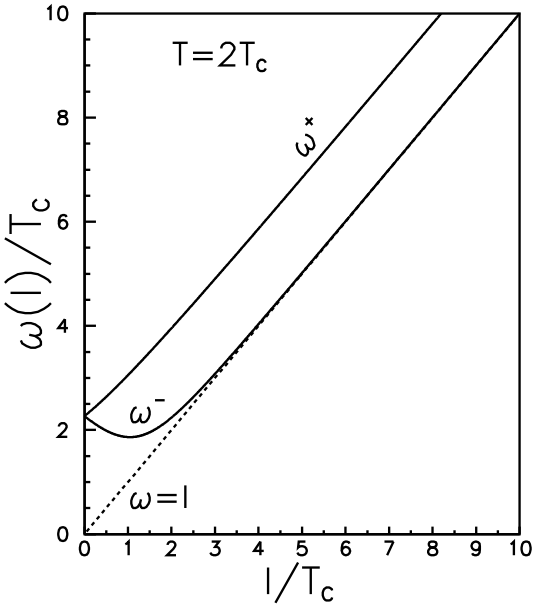

FIG. 2. Quark dispersion relation $\omega(l)/T_c$ versus l/T_c in a QGP at $T = 2\ T_c$ in the presence of a gluon condensate.

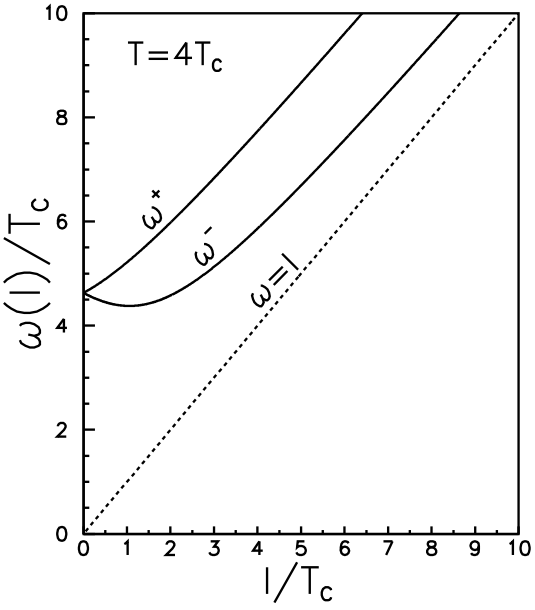

FIG. 3. Quark dispersion relation $\omega(l)/T_c$ versus l/T_c in a QGP at $T = 4\ T_c$ in the presence of a gluon condensate.

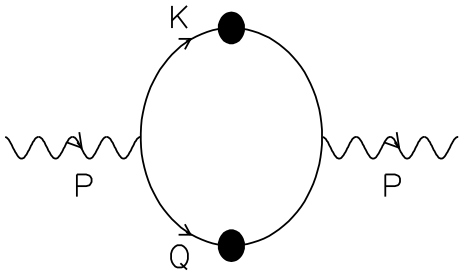

FIG. 4. One-loop photon self energy with effective quark propagators containing the gluon condensate

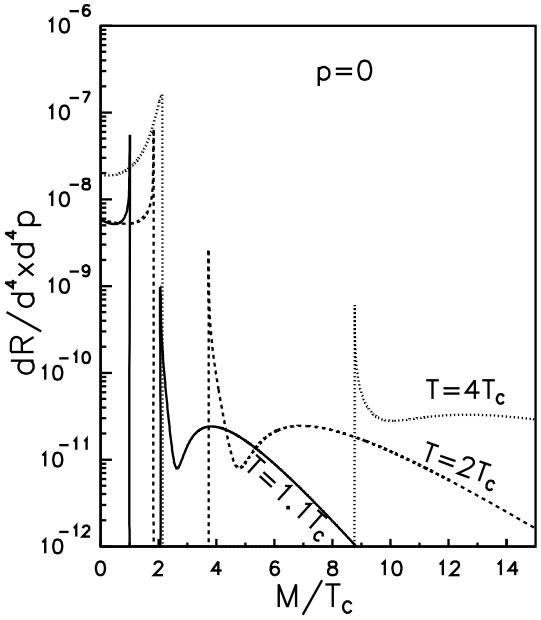

FIG. 5. Dilepton production rate from a QGP in the presence of a gluon condensate at photon momentum $p = 0$.

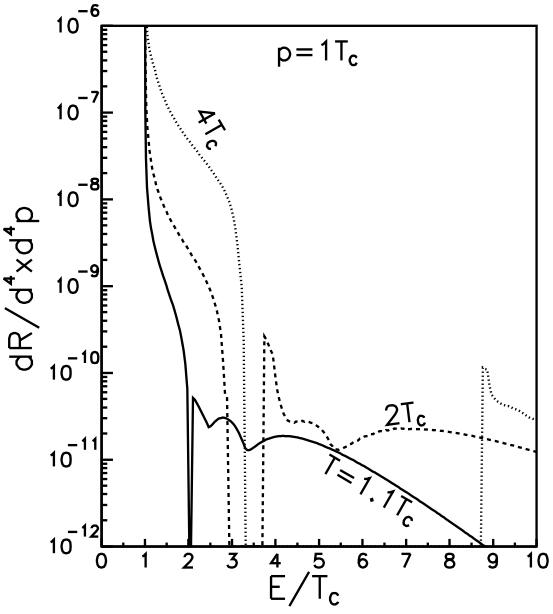

FIG. 6. Dilepton production rate from a QGP in the presence of a gluon condensate at photon momentum $p = 1\ T_c$.

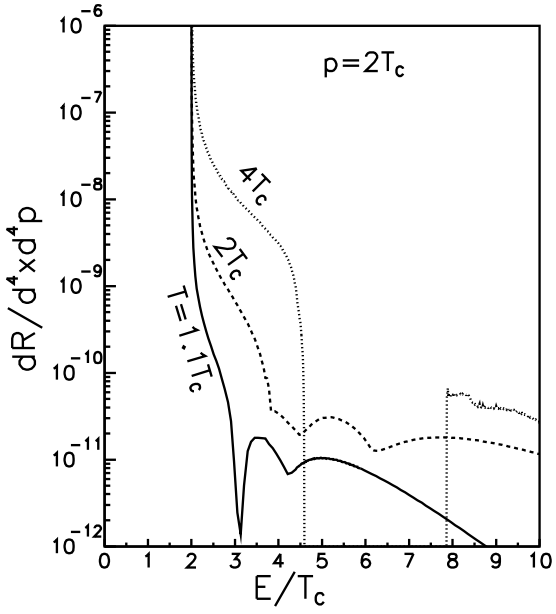

FIG. 7. Dilepton production rate from a QGP in the presence of a gluon condensate at photon momentum $p = 2\ T_c$.

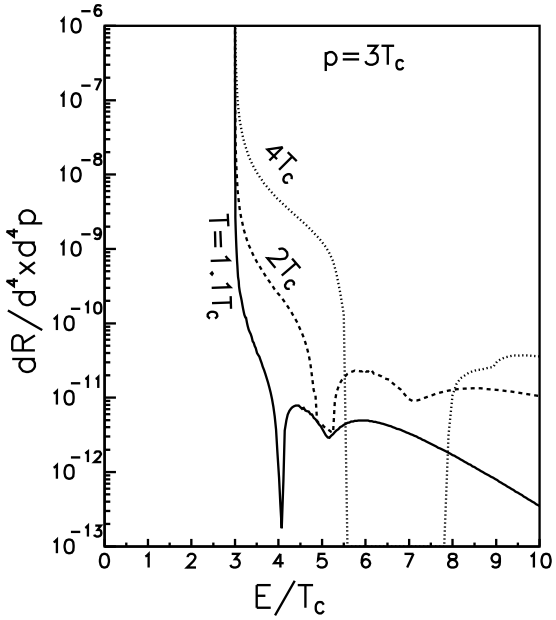

FIG. 8. Dilepton production rate from a QGP in the presence of a gluon condensate at photon momentum $p = 3\ T_c$.